RSC Advances

PAPER

View Article Online
View Journal | View Issue

Cite this: *RSC Adv.*, 2025, **15**, 29119

Effective separation of oil and water mixture using hydrophobic g-C_3N_4 coated natural rubber foam

A. C. Swathi,[a] C. Indhuja[b] and Maneesh Chandran *[a]

Received 15th June 2025
Accepted 11th August 2025

DOI: 10.1039/d5ra04240b

rsc.li/rsc-advances

Frequent oil spills are a major contributor to water pollution, leading to numerous environmental and ecological issues and posing risks of fire and explosions. Hence, there is an imperative to develop a cost-effective and exceptionally functional absorbent material for separating oil and water. In this study, a simple, low-cost, environmentally friendly, biodegradable, highly hydrophobic, and super oleophilic graphitic carbon nitride (g-C_3N_4) based natural rubber foam is introduced for oily wastewater treatment. The g-C_3N_4 was coated onto the natural rubber foam using a simple dip-coating method. The resulting hydrophobic g-C_3N_4-coated foams exhibit highly hydrophobic and superoleophilic surface properties with contact angles of 144.1 ± 2° and 0°, respectively. These foams exhibited more than 100% oil absorption capacity, effectively absorbing a variety of oils and solvents like olive oil, acetone, methanol, ethanol, *etc.* and successfully separating oil and solvent mixtures from water. Hence, the developed g-C_3N_4-based natural rubber foam absorbent has excellent potential for oil/water separation applications.

Introduction

Oil leakage has emerged as a significant global environmental challenge, resulting in the wastage of valuable oil resources and posing serious threats to the safety of marine ecosystems and humans.[1–3] Due to the substantial volume of oily wastewater released from domestic and industrial activities, it is essential to develop and implement efficient, environmentally sustainable methods for the treatment of oily wastewater.[4,5] At present, traditional techniques such as *in situ* burning, bioremediation, sorption, skimming, and chemical dispersants are used for the remediation of oil spills.[6,7] Skimming is the most commonly utilized method for oil/water separation; nevertheless, its practical application remains limited due to low separation efficiency, high operational costs, and prolonged remediation procedures.[8] The second most widely utilized approach involves the application of chemical dispersants. However, the combined toxicity of the dispersant mixture and oils poses significant risks to marine ecosystems.[9] Hence, there is an imperative to develop a cost-effective and highly efficient absorbent material for the separation of oil and water. Recently, there has been significant interest in three-dimensional porous materials, such as organic sponges, metallic foams, and aerogels, which offer large specific surface areas and porosity.[10] These properties make them suitable candidates for the development of super-wettability materials, particularly in applications related to oil/water separation. Nonetheless, bare foams lack the crucial hydrophobic and superoleophilic properties. Consequently, chemical modifications, such as functionalization and nanoparticle impregnation, are necessary for pure foams to be utilized for the separation of oil and water.[11] The primary factors guiding the selection of nanoparticles or nanocomposites for coating on suitable foams are their high absorption capacity, cost-effectiveness, and ease of synthesis.[12]

Among the various adsorbent materials, carbon-based nanoparticle-impregnated absorbents show significant potential for the separation of oil and organic solvents from water. Zhang *et al.* reported CNT/PDMS composite for efficient removal of oil from oil/water mixtures. The prepared foam showed better oil absorption capacity than bare PDMS sponge.[13] Liu *et al.* introduced OTS-CNTs/PU sponge as a potential candidate for oil spill absorption.[14] Krebsz *et al.* present the removal of chromate ions and oil spills from wastewater using bio-graphene foams.[15] Guo *et al.* deposited carbon nanofibers onto the pore walls of the PDMS foam to separate oil from the emulsion.[16] Panicker *et al.* reported amorphous carbon sphere-based superhydrophobic and superoleophilic sponges for oil/water separation.[17] Liu *et al.* developed luffa sponge/graphene composite aerogel incorporated with $CuFe_2O_4$ hollow nanospheres for oil/water separation.[18] Li *et al.* synthesized helical carbon nanofibers for microwave absorption and oil/water separation using chemical vapor deposition method.[19] Yang *et al.* modified polyurethane sponges with stearic acid, polydimethylsiloxane, and multi-walled carbon nanotubes for oil/water separation utilizing photothermal effect.[20] Nevertheless, these methods involve time-consuming and costly synthesis processes, utilizing expensive precursors and equipment.

[a]*National Institute of Technology Calicut, Kerala, 673601, India. E-mail: maneesh@nitc.ac.in*

[b]*St. Joseph's College (Autonomous) Devagiri, Calicut, Kerala, 673008, India*

In this work, we report hydrophobic g-C_3N_4-coated natural rubber foam for oil/water separation for the first time, which is of great interest due to its cost-effective synthesis, high-yield production, effective separation of oil and organic solvents from water and biodegradability. The g-C_3N_4 was synthesized by a simple calcination method,[21] followed by chemical treatment to produce hydrophobic g-C_3N_4. The natural rubber foam was prepared from the milky latex extracted from *Hevea brasiliensis* and a simple dip-coating method was used to produce g-C_3N_4-based rubber foam. The prepared hydrophobic g-C_3N_4-coated foams exhibit high hydrophobicity and superoleophilicity, making them suitable for the treatment of oily wastewater.

Experimental section

Materials

The chemicals utilized in this study were melamine (99%), HDTMS, ethanol, sulphur (S, 99%), potassium oleate (KO, 98%), zinc diethyldithiocarbamate (ZDEC, 99%) and, zinc 2 – mercaptabenzothiazole (ZMBT, 98%), zinc oxide (ZnO, 99%), sodium fluorosilicate (NaFS, 98%), *N*-methyl-pyrrolidone (NMP) and deionized (DI) water. Furthermore, natural rubber latex was used for the synthesis of hydrophobic g-C_3N_4 coated rubber foam. For the oil absorption studies, commercially available engine oil, diesel, toluene, hexane, ethanol, methanol, acetone, and olive oil were used.

Synthesis of hydrophobic g-C_3N_4

The g-C_3N_4 sample was prepared *via* a simple calcination method. A 5 g of melamine was calcinated in a crucible at 550 °C for 2 h in a muffle furnace at a heating rate of 10 °C min^{-1}.[22] After cooling down to ambient temperature, the resultant product was collected and ground into a fine powder. Afterward, 20 mL ethanol and 10 μL of HDTMS were added to a 100 mL beaker and sonicated for 15 min; following this, 200 mg of the g-C_3N_4 was added and again sonicated for 30 min. It was then placed in a hot air oven for 3 h at 90 °C to obtain hydrophobic g-C_3N_4.

Preparation of natural rubber latex foam

The Dunlop method was used for the preparation of natural rubber latex foam.[23] It consists of four processes, namely compounding, foaming, gelling, and vulcanization as schematically shown in Fig. 1. In the first process, 100 mL of natural rubber latex was stirred with a mechanical stirrer for 50 min at 500 rpm to eliminate ammonia, then 3 g of sulphur, 1.5 g of KO, 1 g of ZDEC and, 1 g of ZMBT stirred up to 1 h at 800 rpm, and the mixture was beaten up to 5 min for making it fivefold with a hand blender. Then 5 g ZnO and 1.5 g NaFS (gelling reactants) were added and again beaten up to 2 min to mix it well. The mixture was kept for resting at room temperature for 7 min and vulcanized at 100 °C for 50 min in an oven. Afterward, the non-reactive reagents were removed by washing solid foam with DI water, followed by drying at 40 °C for 12 h.

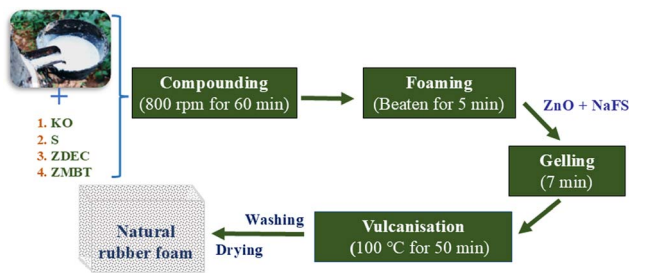

Fig. 1 Schematic diagram for the preparation of natural rubber latex foam.

Preparation of hydrophobic g-C_3N_4 coated natural rubber foam

The hydrophobic g-C_3N_4 coated natural rubber foam was prepared by a simple dip-coating method as schematically shown in Fig. 2. Hydrophobic g-C_3N_4 (0.5 g) was added to 5 mL of NMP, and sonicated for 30 min; subsequently a small piece of natural rubber foam (1 × 1 × 1 cm) was immersed in the mixture and stirred for 2 h using a magnetic stirrer. Then the rubber foam was kept in the oven for 1 h at 90 °C. A thin protective layer was applied to the prepared g-C_3N_4 coated foam to securely embed the hydrophobic g-C_3N_4 particles within the natural rubber foam network. To achieve this, the g-C_3N_4 foam was again dipped in 5 mg mL^{-1} of PVDF/NMP solution for 20 min. Then the foam was again kept in the oven for 12 h at 90 °C.

Oil/water separation method

The manual squeezing method was employed to recover absorbed oils and organic solvents from the natural rubber-based foam after separation from water. The absorbent was gently placed on the surface of the oil–water or solvent–water mixture and allowed to interact until complete absorption of the organic phase was achieved. The absorbent was then carefully removed, and the amount of absorbed oil or solvent was quantified by measuring the weight difference before and after absorption. To recover the absorbed liquid, the sample was placed over a clean glass container and subjected to uniform manual pressure to expel the trapped oil or solvent. Following this, the absorbent was rinsed with deionized water and dried at room temperature prior to further use or characterization.

Characterization

The phase analysis of prepared samples was carried out using an X-ray diffractometer (XRD; Rigaku SmartLab SE). Infrared spectra were recorded using Perkin Elmer-Spectrum Two FTIR spectrometer. The X-ray photoelectron spectroscopy (XPS, Thermo Scientific ESCALAB Xi+) was used to study the surface composition of bare g-C_3N_4 and hydrophobic g-C_3N_4. The microstructures of pure rubber foam and hydrophobic g-C_3N_4 coated natural rubber foam were analyzed using scanning electron microscopy (FESEM; Hitachi SU6600). The static water contact angle (WCA) on g-C_3N_4 coated natural rubber foam using 6 μL water droplets was measured with a contact angle measuring instrument (Holmarc; HO-IAD-CAM-01A). The

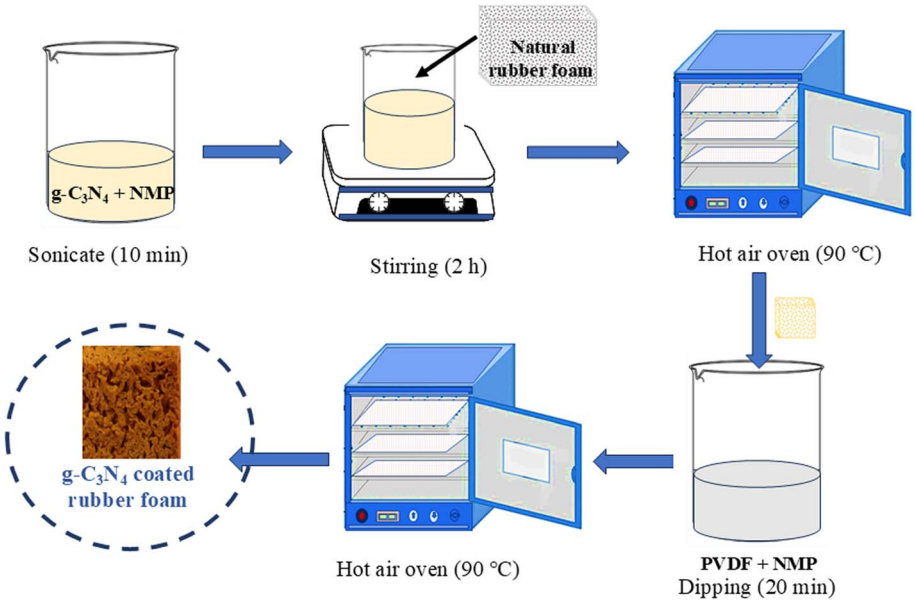

Fig. 2 Schematic diagram for the preparation of hydrophobic g-C_3N_4 coated natural rubber foam.

thermal and mechanical properties of the prepared samples were analysed using a thermogravimetric analyser (TGA; Hitachi-STA7200) and a universal testing machine (UTM; Shimadzu AG-X plus 10 kN).

Results and discussion

XRD analysis

The XRD analyses of the synthesized g-C_3N_4 and hydrophobic g-C_3N_4 are shown in Fig. 3(a). There was no noticeable change in the peak position or in the intensity of peaks after coating with the HDTMS, indicating that the HDTMS layer does not affect the crystalline structure of the g-C_3N_4 phase.[24] The diffraction peak observed at 13°, corresponds to the planar structure of the tri-*s*-triazine unit. Furthermore, the prominent diffraction peak at 27.6° corresponds to the (002) reflection, which is attributed to the graphite-like interlayer stacking of g-C_3N_4.[25,26] Fig. S3 (see SI) shows the XRD pattern of the prepared rubber foam and g-C_3N_4 coated rubber foam, confirming the successful coating of g-C_3N_4 onto the prepared rubber foam network.

FTIR analysis

The FTIR analysis of pure and hydrophobic g-C_3N_4 is shown in Fig. 3(b). The absorption peaks at 887 and 807 cm^{-1} are attributed to the characteristic out-of-plane vibration of triazine or *s*-triazine aromatic repeating units in g-C_3N_4.[27] The absorption band between 1240 and 1640 cm^{-1} corresponds to the stretching vibration of the C–N and C=N in CN aromatic repeating units of g-C_3N_4. Also, a band observed around 3050–3400 cm^{-1} was due to N–H stretching vibrations, indicative of residual amino groups.[28] Upon modification with HDTMS, two new peaks were observed at 2925 and 2852 cm^{-1} in the FTIR spectra of hydrophobic g-C_3N_4.[29,30] These peaks are due to the stretching of methylene groups in the HDTMS chains, which confirmed the successful coating of HDTMS on pure g-C_3N_4.[31]

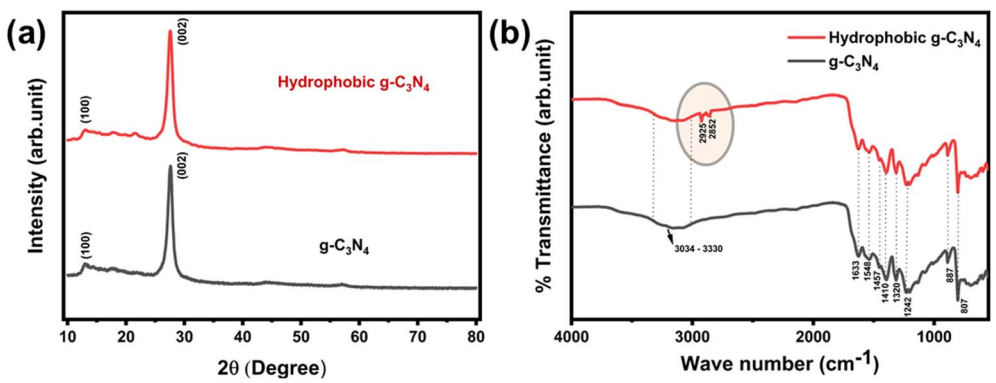

Fig. 3 (a) XRD patterns and (b) FTIR spectra of g-C_3N_4 and hydrophobic g-C_3N_4.

XPS analysis

The surface elemental composition and chemical states of both bare g-C_3N_4 and hydrophobic g-C_3N_4 were characterized using XPS. The XPS survey scan (Fig. 4(a)) revealed the presence of an additional Si signal in the hydrophobic g-C_3N_4 sample that is absent in the bare g-C_3N_4, providing strong evidence for successful coating of HDTMS onto the g-C_3N_4 surface.

High-resolution XP spectra for each element were analysed by fitting with a Voigt function. The C 1s spectrum of hydrophobic g-C_3N_4 (Fig. 4(b)) was well fitted with three components at binding energies of 282.3, 283.1, and 285.8 eV, corresponding to C–C, C–Si, and C–O bonds, respectively.[32] The N 1s spectrum exhibited three distinct peaks at 396.3, 397.3, and 398.7 eV, which are attributed to C–N=C, N–$(C)_3$, and surface uncondensed bridging nitrogen atoms associated with C–N–H functional groups.[33] The O 1s spectrum was best fitted into three peaks at 529.9, 531.3, and 531.4 eV, assigned to Si–O, C–O, and C=O bonds, respectively.[34] The Si 2p spectrum was fitted with two components at 99.9 and 101.0 eV, corresponding to Si and Si–C bonds.[35] In addition to the appearance of Si-related peaks, a pronounced increase in the intensity of C and O characteristic peaks was observed in the hydrophobic g-C_3N_4, further confirming the successful HDTMS modification.

Morphology and surface wettability

The FESEM images of the prepared samples are shown in Fig. 5. In general, the wetting behavior of material surfaces is primarily determined by the surface structure of the sample. Pure natural rubber foam exhibits a porous structure. Upon closer inspection, the surface appears to contain particles, with some cracks observed. The incorporating of g-C_3N_4 onto the rubber foam surface resulted in the formation of micro- and nano-scale protrusions, which significantly enhanced the surface roughness, thereby contributing to the hydrophobic properties of the rubber foam.

The contact angle is a key parameter for studying the wettability of the sample surface. In this study, WCAs were measured on the surface of the prepared samples. The synthesized pristine g-C_3N_4 exhibits hydrophilic property as shown in Fig. 6(a). The g-C_3N_4, when treated with ethanol and HDTMS, exhibited hydrophobic property with average contact angle of 137.8°, as shown in Fig. 6(b). The synthesized pristine natural rubber foam exhibits both hydrophilic and oleophilic nature as shown in Fig. 6(c). Treating the rubber foam with hydrophobic g-C_3N_4 alters its nature, rendering into hydrophobic as shown in Fig. 6(d). The coated rubber showed a superoleophilic nature with an oil contact angle of 0°.

As anticipated, the uncoated natural rubber exhibited significant hydrophilic properties, whereas the hydrophobic g-C_3N_4-coated foam samples exhibited strong water repellence properties, with WCA values >140° (Fig. 6(e)). This change in wettability is attributed to the combined effect of the hydrophobic g-C_3N_4 and fluorine-containing PVDF polymer. Notably, the addition of PVDF polymer resulted in minimal changes in the WCA but contributed to an enhancement in the overall hydrophobicity of g-C_3N_4 foam materials.

Furthermore, the sliding angle of the hydrophobic g-C_3N_4-coated foam was measured, revealing a value less than 10°, which indicates the low adhesion characteristic of the modified surface.

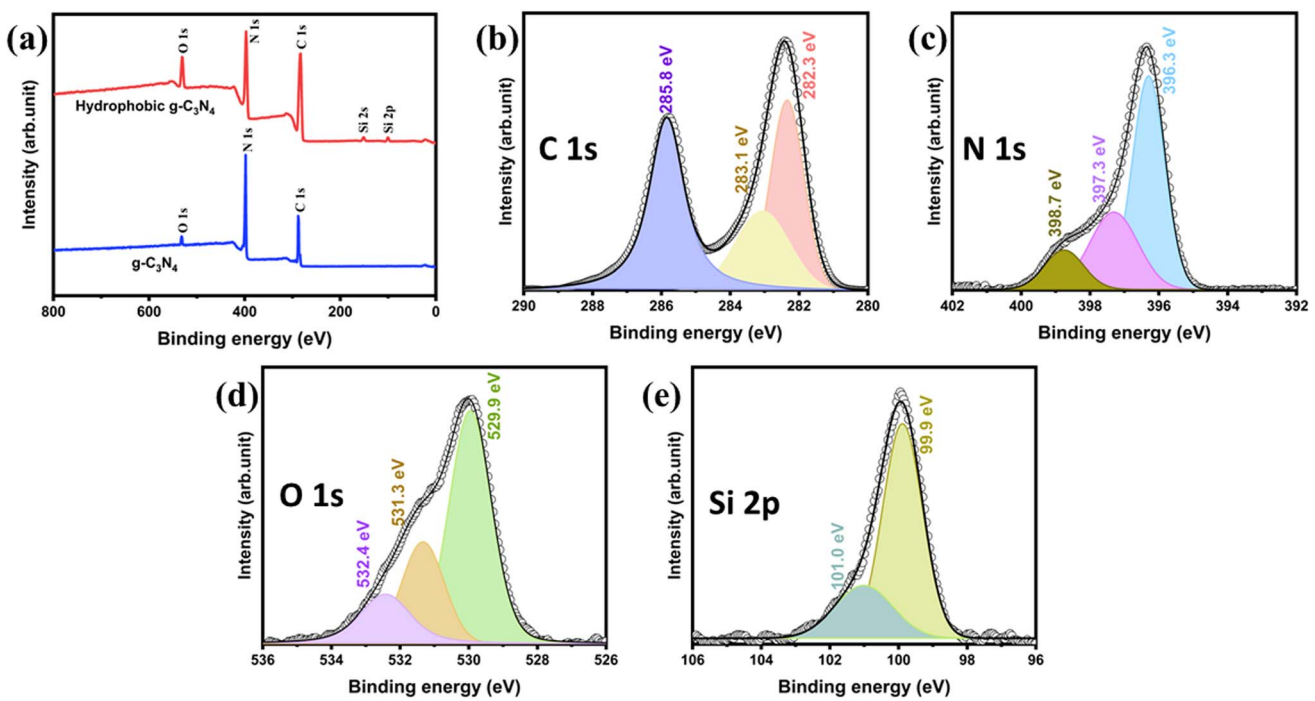

Fig. 4 (a) XPS survey scan of g-C_3N_4 and hydrophobic g-C_3N_4, Narrow scan XPS of hydrophobic g-C_3N_4: (b) C 1s, (c) N 1s, (d) O 1s, and (e) Si 2p.

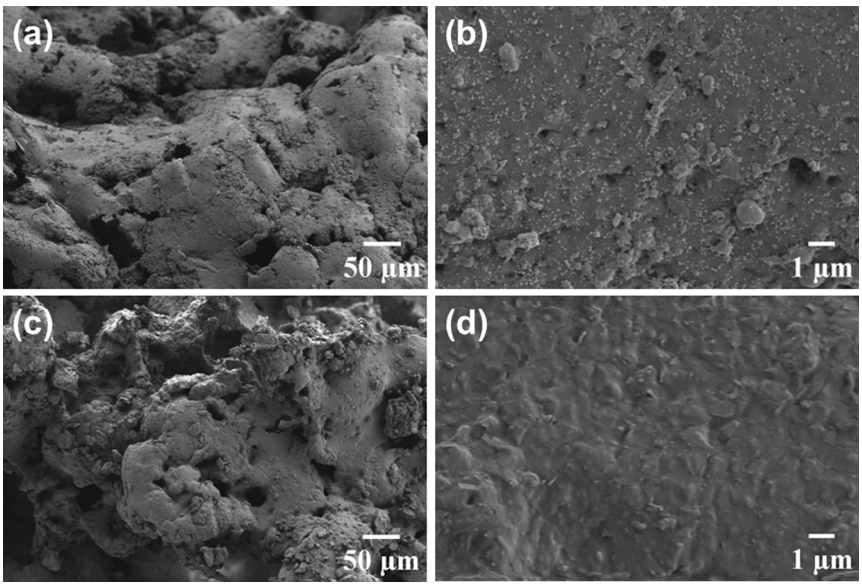

Fig. 5 FESEM images of synthesized (a) and (b) rubber foam and (c) and (d) g-C_3N_4-coated rubber foam samples at different magnifications.

FTIR analysis

To assess whether any chemical alterations occur in the g-C_3N_4 coated natural rubber foam upon oil absorption, FTIR spectra were recorded for the foam both before and after (after cleaning the foam) oil absorption. As depicted in Fig. 7, no noticeable changes were observed in the spectra. The broad peak between 3300 and 3400 cm^{-1} is attributed to the presence of N–H and O–H groups in the sample.[27,36] The absorption bands in the 1200–1640 cm^{-1} are due to stretching modes of C–N rings, while the band near 887 cm^{-1} corresponds to C–H bending vibrations.[36–38] The presence of these characteristic peaks confirms the presence of polyisoprene monomers in natural rubber-based foam. The peaks at 807 cm^{-1} attributed to the stretching vibrations of the triazine ring.[36,39–41] Additionally, other peaks between 2845 cm^{-1} and 2965 cm^{-1}, are corresponding to C–H stretching vibrations in the chains of HDTMS.[30,42–46]

TGA and UTM analysis

For effective real-time applications, the thermal and mechanical stability of prepared g-C_3N_4-coated natural rubber foam was analysed using TGA and UTM. The TGA of the natural rubber foam showed a single stage of mass loss from the temperature range of 325 °C to 450 °C (Fig. 8(a)). There was no significant thermal degradation detected at temperatures below 300 °C, which is attributed to the scission and crosslinking of carbon

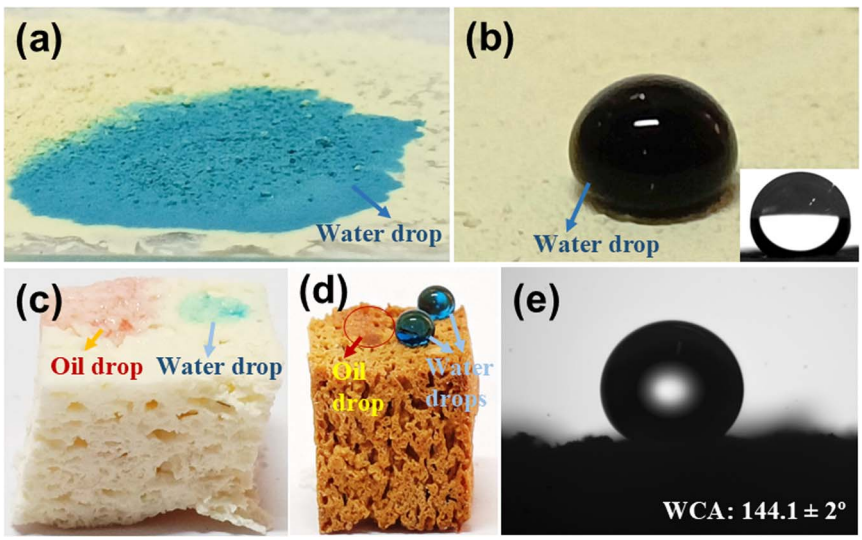

Fig. 6 (a) Hydrophilic nature of pristine g-C_3N_4, (b) hydrophobic nature of g-C_3N_4, inset shows hydrophobic g-C_3N_4 with WCA with 137.8°. Oil and water droplets on (c) natural rubber foam and (d) hydrophobic g-C_3N_4 coated natural rubber foam with (e) WCA 144.1 ± 2°.

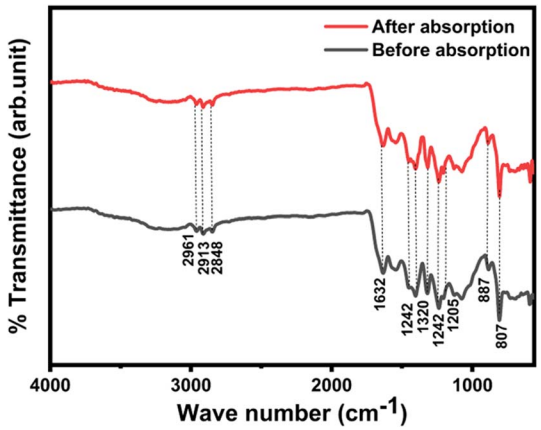

Fig. 7 FTIR spectra of the foam material before oil absorption and after cleaning following oil absorption.

chains within the rubber foam molecules.[47–49] These processes do not lead to significant volatility loss in the rubber foam. The TGA of the hydrophobic g-C_3N_4 coated foam exhibits minimal variation, which can be attributed to the addition of g-C_3N_4 into the foam surface. The compression study also showed good mechanical strength of our prepared foams (Fig. 8(b)).

Oil/water mixture separation performance

The efficiency of oil/water separation is primarily influenced by the surface wettability of the adsorbent materials. As mentioned, the hydrophobic g-C_3N_4 coated natural rubber foam was prepared using a simple dip-coating technique. The particle loading percentage was calculated using eqn (1),

$$\text{Particle loading}\% = \frac{W_{RG} - W_R}{W_R} \times 100\% \quad (1)$$

where W_{RG} and W_R represent the weights of the hydrophobic g-C_3N_4 loaded foam and the uncoated natural rubber foam, respectively.[50] At an optimal nanoparticle loading of ~13.6%, the water droplet exhibits a spherical shape, with a WCA of 144.1 ± 2°, along with a high oil absorption capacity. Increasing the nanoparticle concentration beyond this optimal point enhances the WCA (Fig. 9(a)); nonetheless, it concurrently reduces the oil absorption capacity of the foam. This reduction can be attributed to the accumulation of nanoparticles within the foam's pore structure. Upon the application of an external force to dip the hydrophobic g-C_3N_4-coated foam in water, a silver colour appeared on the surface of the foam (Fig. 9(b)), resulting from the foam's high surface roughness.[51,52] Fig. 9(c)–(f) illustrate the efficient separation of oil from water using the hydrophobic g-C_3N_4 coated natural rubber foam. The foam rapidly absorbed oil within 5 s upon contact with oil-contaminated water, demonstrating its capacity to effectively remove oil. Therefore, the hydrophobic g-C_3N_4-coated natural rubber foam exhibits significant potential for oil absorption applications.

To evaluate the durability of hydrophobic g-C_3N_4 coated foam in a corrosive environment, the absorbent material was immersed in aqueous solutions with various pH conditions. Even after 20 h of exposure, the foam retained its water–repellent properties. Post-exposure in various pH environments, WCAs were measured to determine any changes in surface wettability, as shown in Fig. 10(a). The results revealed a slight decrease in WCA values; yet, the foam retained its hydrophobic properties. The g-C_3N_4 exhibited a highly inert adsorbent surface in terms of chemical reactivity.[53] The hydrophobic g-C_3N_4 coated foam possesses significant chemical resistance and can perform effectively in any harsh conditions.

Additionally, the variation in WCA over a period of 0–60 days of exposure to air is depicted in Fig. 10(b). After 60 days, the WCA of the foam decreased only slightly from 144.1 ± 2° to 141.8 ± 2°, demonstrating remarkable long-term stability. The sustained superhydrophobicity of hydrophobic g-C_3N_4 coated foam is attributed to the strong adhesion of PVDF and the robust chemical stability of the g-C_3N_4, which together maintain a low surface energy on the natural rubber foam substrate. Thus, the hydrophobic g-C_3N_4 coated natural rubber foam emerges as a promising material for practical applications.

An effective absorber must exhibit both high absorption capacity and recyclability. In this study, the absorption capacity and recyclability of the hydrophobic g-C_3N_4-coated natural rubber foams were assessed through the manual squeezing method. This method involves immersing and manually

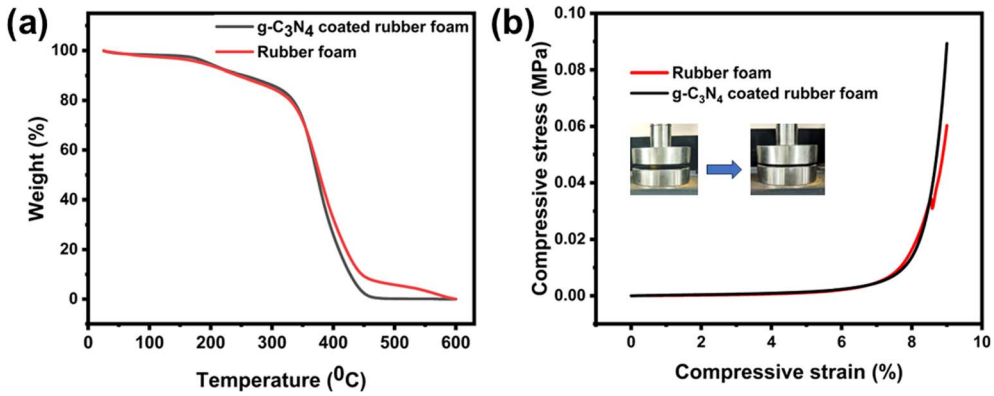

Fig. 8 (a) TGA and (b) stress–strain curve for rubber foam and g-C_3N_4 coated rubber foam.

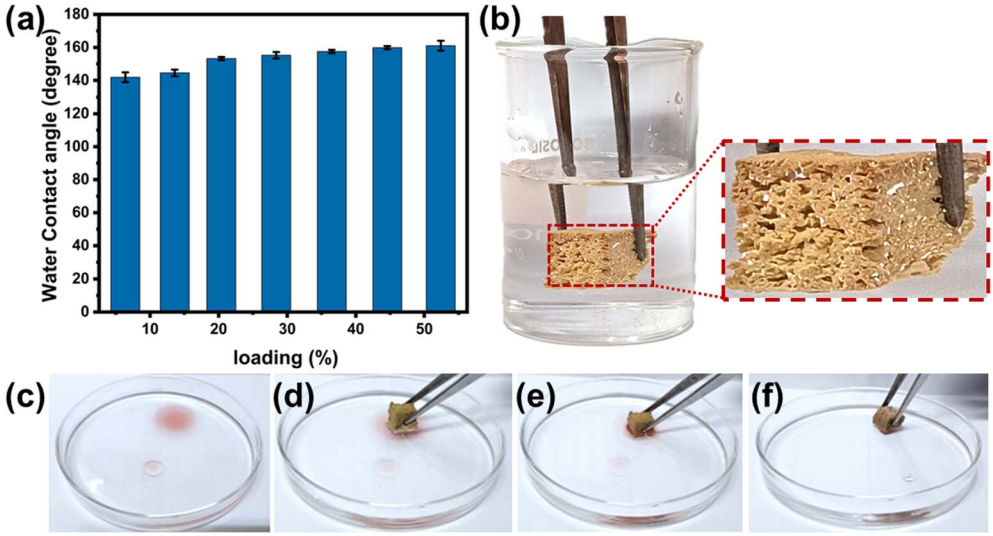

Fig. 9 (a) Water contact angle obtained for various amount of hydrophobic g-C_3N_4 nanoparticle loadings in the natural rubber foam. (b) Photographs of the hydrophobic g-C_3N_4 coated foam immersed in water. (c)–(f) Present a sequential photograph illustrating the process of oil removal from water utilizing the hydrophobic g-C_3N_4 coated natural rubber foam.

squeezing the foam to release the absorbed liquids, offering a sustainable and time-efficient alternative to burn-off techniques. The absorption capacity of organic solvents and oils is governed by their physicochemical properties, such as viscosity, density, and surface tension. The hydrophobic g-C_3N_4-coated natural rubber foam exhibited more than 100% absorption capacity for almost all tested oils and organic solvents. These results are better than previous reports on oil–water separation, as shown in Table 1. Notably, the g-C_3N_4-coated foam demonstrated superior chloroform separation performance compared to other solvents such as engine oil, diesel, toluene, hexane, ethanol, methanol, acetone, and olive oil (see Fig. 11(a)). The absorption capacity of the foam was quantified by the weight gain ratio, calculated using eqn (2).

$$\text{Absorption capacity}(\%) = \frac{M_2 - M_1}{M_1} \times 100 \quad (2)$$

where M_1 and M_2 represent the weights of the hydrophobic g-C_3N_4-coated natural rubber foam before and after the absorption of oils or organic solvents, respectively.

The surface modification of the natural rubber foam with g-C_3N_4 significantly enhanced the separation efficiency for all tested oils, indicating its broad applicability and efficacy in oil removal systems. The recyclability of the foam was assessed using chloroform, toluene, and engine oil through the manual squeezing method. The results indicated that efficient separation was achieved for up to 25 cycles without significant material degradation, as shown in Fig. 11(b). The hydrophobic g-C_3N_4-coated natural rubber foam demonstrated outstanding absorption recyclability for both organic solvents and oils. The foam maintained its hydrophobicity for >25 cycles, after which the WCA decreased to approximately 112°. Nevertheless, the overall oil absorption performance remained unaffected, as shown in Fig. 11(b). The observed reduction in oil absorption was due to the incomplete removal of residual oil during the manual squeezing process. Overall, the hydrophobic g-C_3N_4-coated natural rubber foam has excellent recyclability.

The critical surface energy (γ_c) of the hydrophobic g-C_3N_4-coated natural rubber foam was quantified using the Zisman

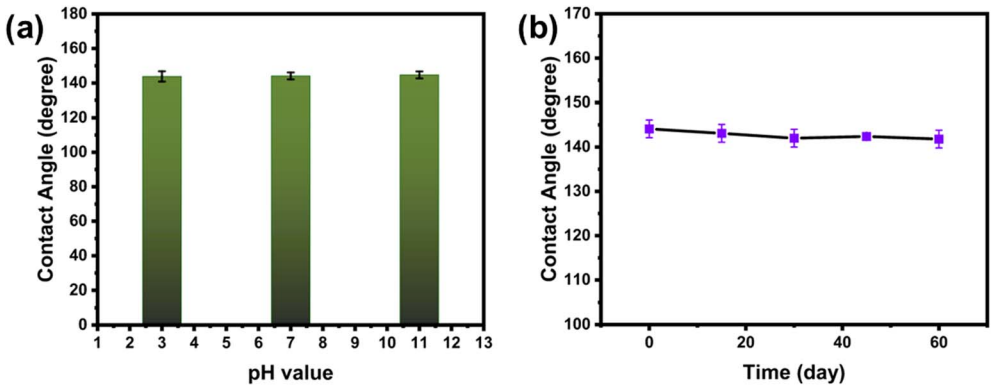

Fig. 10 (a) Stability assessment of the hydrophobic g-C_3N_4-coated natural rubber foam after 20 h of in aqueous solutions with different pH values. (b) Changes in WCA of the hydrophobic g-C_3N_4-coated natural rubber foam over an exposure period ranging from 0 to 60 days in air.

Table 1 Comparative evaluation of hydrophobic g-C_3N_4 coated foam and other adsorbent materials in oil–water separation studies

Sorbents	WCA (°)	Maximum absorption capacity (%)	Reference
PDMS@SiO_2@WS_2 sponge	158.8 ± 1.4	22–112	54
PPy-PA PU sponge	140	22–62	55
Twisted carbon fiber aerogel	—	50–192	56
Carbon nanotube sponges	156	80–180	57
Silylated wood sponge	151	16–41	58
Carbon soot sponge	144	80	59
Starch@PDMS@PU	157.7 ± 2.4	46	60
Hydrophobic g-C_3N_4 coated foam	144.1 ± 2	101–732	This work

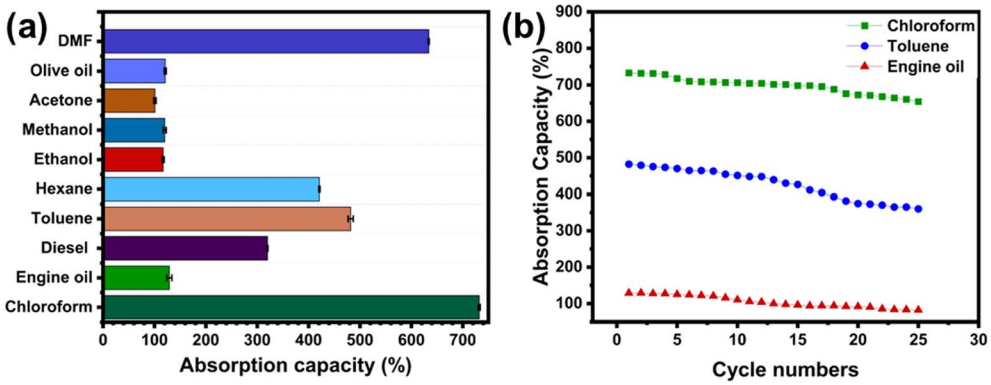

Fig. 11 (a) The absorption capacity of hydrophobic g-C_3N_4-coated natural rubber foam with different organic solvents and oils. (b) Recyclability of hydrophobic g-C_3N_4-coated natural rubber foam for oil recovery was assessed through a manual squeezing method.

analysis by plotting cos θ *versus* liquid surface tension (γ) for various solvents. The γ_c represents the surface tension at or below which complete wetting occurs (contact angle $\theta = 0°$, cos $\theta = 1$).[17,61] To obtain γ_c, contact angles were measured by dropping 6 μL of different test liquids onto the foam surface, and then plotted cosine of the contact angle as a function of γ, as shown in Fig. 12. This result indicates that solvents with surface tensions ≤37 mN m^{-1} can be completely absorbed by the foam. So, the synthesized hydrophobic g-C_3N_4-coated natural rubber foam demonstrates strong potential for efficient oil/water separation applications.

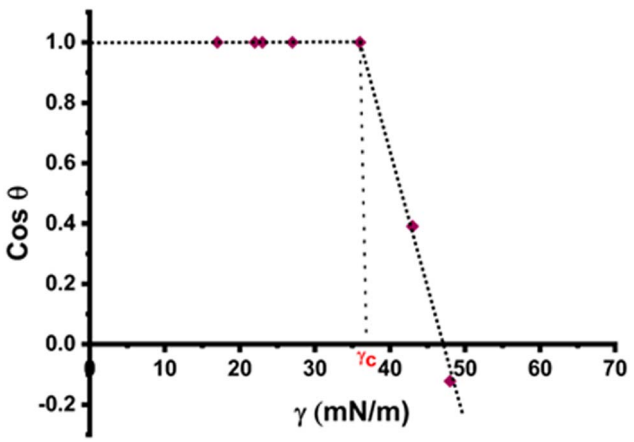

Fig. 12 Zisman plot to determine the critical surface tension of wetting for the hydrophobic g-C_3N_4-coated natural rubber foam in the presence of various organic solvents.

The recovering oil from emulsions is of significant importance in various industrial applications and environmental processes, particularly in water treatment. To assess the separation efficiency of the hydrophobic g-C_3N_4-coated natural rubber foam, a surfactant-stabilized toluene-in-water emulsion was used for testing, along with sodium dodecyl sulfate (SDS) as a surfactant. Upon treatment with g-C_3N_4-coated natural rubber foam, the emulsion undergoes destabilization, leading to effective demulsification. The demulsification observed in this study can be primarily attributed to the intermolecular interactions between the emulsion droplets and hydrophobic g-C_3N_4-coated natural rubber foam. Specifically, these interactions involve both attractive forces toward the oil phase and repulsive forces against the aqueous phase.[62–64] The contact between the modified foam and the emulsion significantly lowers the interfacial tension at the oil–water interface, thereby facilitating the selective absorption of the dispersed toluene droplets into the foam matrix.[65,66] Simultaneously, the continuous aqueous phase is repelled due to the hydrophobic nature of the foam surface. Consequently, the toluene phase is efficiently separated through the foam, yielding a clear and transparent aqueous filtrate (see Fig. 13). This result demonstrates that the prepared foam exhibits excellent demulsification performance.

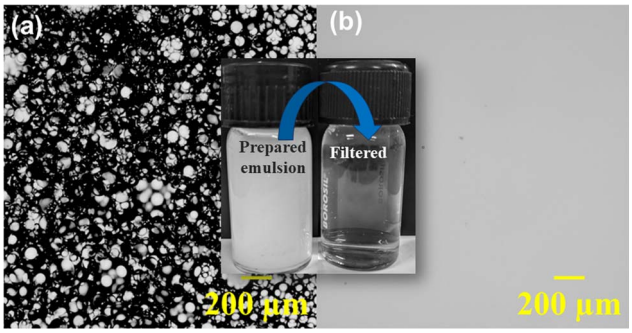

Fig. 13 Optical images of the prepared oil-in-water emulsion: (a) before and (b) after separation.

Conclusions

The development of hydrophobic g-C_3N_4-coated natural rubber foam presents a promising step toward sustainable oil/water separation technologies. The foam, prepared *via* the Dunlop method followed by low-temperature dip-coating, is biodegradable, cost-effective, and suitable for scalable production. The g-C_3N_4 coating imparts near-superhydrophobicity, with a static water contact angle exceeding 140°, and enables efficient separation of both oil/water mixtures and surfactant-stabilized emulsions.

While the study demonstrates excellent performance under batch conditions, further evaluation in continuous flow systems and a detailed assessment of long-term reusability and biodegradability are needed. Despite these limitations, the g-C_3N_4-coated natural rubber foam offers a practical, eco-friendly solution with strong potential for real-world applications such as industrial wastewater treatment and oil spill remediation.

Conflicts of interest

The authors declare no conflicts of interest.

Data availability

The data supporting this study are provided in the SI. The supplementary materials include schematic diagram for the preparation of hydrophobic g-C_3N_4, XRD data, photographs of the synthesized samples, as well as the oil removal capacity of the prepared sample (Fig. S1–S5 and Video S6). See DOI: **https://doi.org/10.1039/d5ra04240b**.

Acknowledgements

The authors sincerely acknowledge the Department of Physics, National Institute of Technology Calicut, for providing access to the XRD facility (FIST, Grant no. SR/FST/PSI-113/2019) and the FTIR facility. Additionally, the authors are grateful to the Optofluidics and Interface Science Laboratory for optical imaging of the samples. The support from the Departments of Chemical Engineering, Chemistry, and Materials Science and Engineering for TGA, UTM, contact angle measurements, and SEM facilities is also acknowledged.

References

1 X. Ye, B. Zhang, K. Lee, R. Storesund, X. Song, Q. Kang, P. Li and B. Chen, *J. Hazard. Mater.*, 2024, **469**, 133832.
2 Y. Han, I. M. Nambi and T. Prabhakar Clement, *Sci. Total Environ.*, 2018, **626**, 795–806.
3 A. Abidli, Y. Huang, P. Cherukupally, A. M. Bilton and C. B. Park, *Environ. Technol. Innovat.*, 2020, **18**, 100598.
4 F. Chen, J. Song, Z. Liu, J. Liu, H. Zheng, S. Huang, J. Sun, W. Xu and X. Liu, *ACS Sustainable Chem. Eng.*, 2016, **4**, 6828–6837.
5 S. Mirshahghassemi and J. R. Lead, *Environ. Sci. Technol.*, 2015, **49**, 11729–11736.
6 Z. Xue, Y. Cao, N. Liu, L. Feng and L. Jiang, *J. Mater. Chem. A*, 2014, **2**, 2445–2460.
7 Y. Yang, H. Wang, J. Li, B. He, T. Wang and S. Liao, *Environ. Sci. Technol.*, 2012, **46**, 6815–6821.
8 Z. Shi, W. Zhang, F. Zhang, X. Liu, D. Wang, J. Jin and L. Jiang, *Adv. Mater.*, 2013, **25**, 2422–2427.
9 A. Shome, K. Maji, A. M. Rather, A. Yashwanth, D. K. Patel and U. Manna, *Chem. Asian J.*, 2019, **14**, 4732–4740.
10 Y. Guan, F. Cheng and Z. Pan, *Polymers*, 2019, **11**, 806.
11 N. Y. Abu-Thabit, O. J. Uwaezuoke and M. H. Abu Elella, *Chemosphere*, 2022, **294**, 133644.
12 J. Li, M. Tenjimbayashi, N. S. Zacharia and S. Shiratori, *ACS Sustainable Chem. Eng.*, 2018, **6**, 10706–10713.
13 W. Zhang, J. Wang, X. Han, L. Li, E. Liu and C. Lu, *Materials*, 2021, **14**, 2431.
14 D. Liu, S. Wang, T. Wu and Y. Li, *Nanomaterials*, 2021, **11**, 3344.
15 M. Krebsz, T. Pasinszki, T. T. Tung, M. J. Nine and D. Losic, *Chemosphere*, 2021, **263**, 127790.
16 Z. Guo, B. Long, S. Gao, J. Luo, L. Wang, X. Huang, D. Wang, H. Xue and J. Gao, *J. Hazard. Mater.*, 2021, **402**, 123838.
17 R. Panickar, C. B. Sobhan and S. Chakravorti, *Langmuir*, 2021, **37**, 12501–12511.
18 Z. Liu, B. Gao, P. Zhao, H. Fu and A. R. Kamali, *Sep. Purif. Technol.*, 2024, **337**, 126347.
19 Y. Li, S. Guo, L. Zhao, S. Chen, Y. Li, X. Yang, P. Wang, W. Feng, Z. Mou, H. Jiang, H. Wei and G. Cerullo, *Carbon*, 2025, **233**, 119923.
20 G. Yang, Y. Zhang, Z. Yin, Y. Deng, Z. Li, Y. Xie, Y. Chen, C. Yang, H. Yang, Y. Luo, Z. Hong and M. Xue, *Fuel*, 2025, **381**, 133353.
21 A. C. Swathi, S. T. Sandhiya, S. B and M. Chandran, *Chemosphere*, 2024, **350**, 141013.
22 K. Maślana, T. Kędzierski, A. Żywicka, B. Zielińska and E. Mijowska, *Environ. Nanotechnol. Monitor. Manage.*, 2022, **17**, 100656.
23 B. Sukkaneewat and S. Utara, *Ultrason. Sonochem.*, 2022, **82**, 105873.
24 N. Agrawal, J. S. J. Tan, P. S. Low, E. W. M. Fong, Y. Lai and Z. Chen, *Adv. Mater. Inter.*, 2019, **6**, 1900032.

25 X. Bai, L. Wang, R. Zong and Y. Zhu, *J. Phys. Chem. C*, 2013, **117**, 9952–9961.
26 A. C. Swathi and M. Chandran, *J. Appl. Phys.*, 2023, **133**, 204905.
27 T. Narkbuakaew and P. Sujaridworakun, *Top. Catal.*, 2020, **63**, 1086–1096.
28 S. Pareek, M. Sharma, S. Lal and J. K. Quamara, *J. Mater. Sci.: Mater. Electron.*, 2018, **29**, 13043–13051.
29 B. Xu and Q. Zhang, *ACS Omega*, 2021, **6**, 9764–9770.
30 S. Fan, S. Jiang, Z. Wang, P. Liang, W. Fan, K. Zhuo and G. Xu, *Nanomaterials*, 2022, **12**, 2510.
31 H. Pang, Y. Qiu and W. Sheng, *Sci. Rep.*, 2023, **13**, 5531.
32 Q. Chen, Y. He, S. Yan, H. Zhou, H. Li, Z. Li, K. Wei, W. Chen, J. Yan, G. Wu and X. Yuan, *J. Solid State Electrochem.*, 2023, **27**, 3583–3595.
33 Y. Lin, L. Wang, Y. Yu, X. Zhang, Y. Yang, W. Guo, R. Zhang, Y. Zhai and Y. Liu, *New J. Chem.*, 2021, **45**, 18598–18608.
34 S. Cao, S. Cheng, P. Wang, S. Ge, L. Cai and J. Cai, *Colloid Interface Sci. Commun.*, 2023, **57**, 100757.
35 A. Kaur, P. Chahal and T. Hogan, *IEEE Electron Device Lett.*, 2016, **37**, 142–145.
36 H. Li, Y. Jing, X. Ma, T. Liu, L. Yang, B. Liu, S. Yin, Y. Wei and Y. Wang, *RSC Adv.*, 2017, **7**, 8688–8693.
37 S. Pareek, M. Sharma, S. Lal and J. K. Quamara, *J. Mater. Sci.: Mater. Electron.*, 2018, **29**, 13043–13051.
38 I. Benisti, F. Shaik, Z. Xing, A. Ben-refael, L. Amirav and Y. Paz, *Appl. Surf. Sci.*, 2021, **542**, 148432.
39 D. Liu, C. Lu and J. Wu, *J. Nanopart. Res.*, 2018, **20**, 277.
40 L. He, X. Qi, W. Wei, X. Zhang, J. Wang and Z. Gao, *J. Hazard. Mater.*, 2024, **477**, 135222.
41 W. Li, Q. Chen and Q. Zhong, *J. Mater. Sci.*, 2020, **55**, 10712–10724.
42 C. Fan, J. Miao, G. Xu, J. Liu, J. Lv and Y. Wu, *RSC Adv.*, 2017, **7**, 37185–37193.
43 M. Vidale, O. Craig, F. Desset, G. Guida, P. Bianchetti, G. Sidoti, M. Mariottini and E. Battistella, *Iran*, 2012, **50**, 27–44.
44 S. Deng, Z. Yang, G. Lv, Y. Zhu, H. Li, F. Wang and X. Zhang, *Appl. Phys. A*, 2019, **125**, 44.
45 D. Xia, W. Wang, R. Yin, Z. Jiang, T. An, G. Li, H. Zhao and P. K. Wong, *Appl. Catal., B*, 2017, **214**, 23–33.
46 G. Sui, W. H. Zhong, X. P. Yang and Y. H. Yu, *Mater. Sci. Eng., A*, 2008, **485**, 524–531.
47 S. Phomrak, A. Nimpaiboon, B. Z. Newby and M. Phisalaphong, *Polymers*, 2020, **12**, 1959.
48 M. Reowdecha, P. Dittanet, P. Sae-oui, S. Loykulnant and P. Prapainainar, *Heliyon*, 2021, **7**, e07176.
49 U. Moonart and S. Utara, *Cellulose*, 2019, **26**, 7271–7295.
50 S. Luo, N. Liu, J. Li, C. Gao, J. Sun, Y. Wang, L. Zhang, L. Song, S. Huang, J. Li and S. He, *J. Porous Mater.*, 2023, **30**, 141–148.
51 S. Banerjee, *arXiv*, 2008, preprint, arXiv:arXiv:0808.1460, DOI: **10.48550/arXiv.0808.1460**, **https://arxiv.org/abs/0808.1460**.
52 X. Zhang, W. Zhu, G. He, P. Zhang, Z. Zhang and I. P. Parkin, *J. Mater. Chem. A*, 2016, **4**, 14180–14186.
53 R.-H. Gao, Q. Ge, N. Jiang, H. Cong, M. Liu and Y.-Q. Zhang, *Front. Chem.*, 2022, **10**, 1048504.
54 G. Zhai, L. Qi, W. He, J. Dai, Y. Xu, Y. Zheng, J. Huang and D. Sun, *Environ. Pollut.*, 2021, **269**, 116118.
55 M. Khosravi and S. Azizian, *ACS Appl. Mater. Interfaces*, 2015, **7**, 25326–25333.
56 H. Bi, Z. Yin, X. Cao, X. Xie, C. Tan, X. Huang, B. Chen, F. Chen, Q. Yang, X. Bu, X. Lu, L. Sun and H. Zhang, *Adv. Mater.*, 2013, **25**, 5916–5921.
57 X. Gui, J. Wei, K. Wang, A. Cao, H. Zhu, Y. Jia, Q. Shu and D. Wu, *Adv. Mater.*, 2010, **22**, 617–621.
58 H. Guan, Z. Cheng and X. Wang, *ACS Nano*, 2018, **12**, 10365–10373.
59 Y. Gao, Y. S. Zhou, W. Xiong, M. Wang, L. Fan, H. Rabiee-Golgir, L. Jiang, W. Hou, X. Huang, L. Jiang, J.-F. Silvain and Y. F. Lu, *ACS Appl. Mater. Interfaces*, 2014, **6**, 5924–5929.
60 Y. Li, J. Li, Y. Lu, W. Shi and H. Tian, *Polymer*, 2022, **262**, 125505.
61 A. K. Roy Choudhury, in *Principles of Textile Finishing*, Elsevier, 2017, pp. 149–194.
62 J. Wang, H. Wang and G. Geng, *Mar. Pollut. Bull.*, 2018, **127**, 108–116.
63 D. Langevin, *Langmuir*, 2023, **39**, 3821–3828.
64 R. Liu, J. Gao, Y. Liu, W. Zhang, T. Wu and Y. Li, *J. Cleaner Prod.*, 2024, **449**, 141694.
65 D. Lang, G. Liu, R. Wu, G. Chen, C. Zhang, C. Yang, W. Wang, J. Wang and J. Fu, *Chem. Eng. J.*, 2023, **471**, 144752.
66 Y. Gao, X. Yan, Y. Chen, Y. Sui, N. Wang, T. Wang and G. Gao, *J. Hazard. Mater.*, 2025, **488**, 137486.